

# The Complex X-ray Spectrum of 3C 273: *ASCA* Observations

M. Cappi<sup>1,2</sup>, M. Matsuoka<sup>1</sup>, C. Otani<sup>1</sup> & K.M. Leighly<sup>1,3</sup>

<sup>1</sup> The Institute of Physical and Chemical Research (RIKEN),  
Hirosawa 2-1, Wako, Saitama 351-01, Japan

<sup>2</sup> Istituto per le Tecnologie e Studio Radiazioni Extraterrestri (ITeSRE), CNR,  
Via Gobetti 101, I-40129 Bologna, Italy

<sup>3</sup> Columbia Astrophysics Laboratory, Columbia University,  
538 West 120th Street, New York, NY 10027

Accepted for publication in P.A.S.J.

Received \_\_\_\_\_; accepted \_\_\_\_\_

## ABSTRACT

Results obtained from 9 X-ray observations of 3C 273 performed by *ASCA* are presented (for a total exposure time of about 160 000 s). The analysis and interpretation of the results is complicated by the fact that 4 of these observations were used for on-board calibration of the CCDs spectral response. In particular, we had to pay special attention to the low energy band and 5–6 keV energy range where systematic effects could distort a correct interpretation of the data.

The present standard analysis shows that, in agreement with official recommendations, a conservative systematic error (at low energies) of  $\sim 2\text{--}3 \times 10^{20} \text{ cm}^{-2}$  must be assumed when analyzing *ASCA* SIS data. A soft-excess, with variable flux and/or shape, has been clearly detected as well as flux and spectral variability that confirm previous findings with other observatories. An anti-correlation is found between the spectral index and the flux in the 2-10 keV energy range. With the old response matrices, an iron emission line feature with EW  $\sim 50\text{--}100$  eV was initially detected at  $\sim 5.6\text{--}5.7$  keV ( $\sim 6.5\text{--}6.6$  keV in the quasar frame) in 6 observations and, in two occasions, the line was resolved ( $\sigma \sim 0.2\text{--}0.6$  keV). Comparison with the Crab spectrum indicates however that this feature was mostly due to remaining calibration uncertainties between 5–6 keV. Indeed, fitting the data with the latest publicly available calibration matrices, we find that the line remains unambiguously significant in (only) the two observations with lowest fluxes where it is weak (EW  $\sim 20\text{--}30$  eV), narrow and consistent with being produced by Fe  $K_{\alpha}$  emission from neutral matter.

Overall, the observations are qualitatively consistent with a variable, non-thermal X-ray continuum emission, i.e., a power law with  $\Gamma \sim 1.6$  (possibly produced in the innermost regions of the radio-optical jet), plus underlying “Seyfert-like” features, i.e., a soft-excess and Fe  $K_{\alpha}$  line emission. The data are consistent with some contribution (up to a few 10% level in the *ASCA* energy band) from a “Seyfert-like” direct continuum emission, i.e. a power law with  $\Gamma \sim 1.9$  plus a reflection component, as well. When the continuum (jet) emission is in a low state, the spectral features produced by the Seyfert-like spectrum (soft-excess, iron line and possibly a steep power law plus a reflection continuum) are more easily seen.

*Subject headings:* galaxies: active — galaxies: individual (3C 273)

## 1. Introduction

The remarkable discovery by EGRET on-board *CGRO* that blazars (i.e. BL Lacertae objects and flat-spectrum radio quasars) are strong  $\gamma$ -ray emitters has drawn in recent years the attention of the astronomical community to this class of objects. Observations indicate that the overall energy distribution of blazars shows the signature of two different types of emission mechanisms: beamed non-thermal jet radiation producing the overall broad band (from radio to  $\gamma$ -rays) continuum emission common to all blazars, and quasi-isotropic thermal radiation by an accretion-disk producing a “UV Bump” observed in a large number of quasars and Seyfert galaxies but absent in BL Lac objects (e.g. Sambruna, Maraschi & Urry, 1996, Elvis et al. 1994). The non-thermal continuum consists of IR-optical and  $\gamma$ -ray peaks. The first peak is interpreted in terms of synchrotron emission and the second peak in terms of inverse Compton emission (see Urry & Padovani 1995 for a review on the subject). From object to object, the observed different spectral characteristics may be due to the relative importance of one emission mechanism to the other which, in turn, is likely to be related to the amount of beaming in one object or the other (e.g. Dondi & Ghisellini 1995).

One of the most well-studied and characteristic example of blazars is the bright quasar 3C 273 ( $z \simeq 0.158$ ). It is a good example where both non-thermal and thermal emission mechanisms might be observed because its broad band energy distribution exhibits two large peaks, one peaking in the IR-optical and one peaking in the  $\gamma$ -rays with a ‘UV bump’ superimposed on it (Courvoisier et al. 1987, Lichti et al. 1995, von Montigny et al. 1997). The study of its X-ray properties may provide important clues to understand the origin of both emission mechanisms because a) soft-X-ray excess emission has been observed and interpreted as the high-energy tail of the UV bump (Turner et al. 1985, Courvoisier et al. 1987, Walter et al. 1994, Leach, Mc Hardy & Papadakis 1995) and b) the 2-10 keV spectrum which is most likely associated to the  $\gamma$ -ray emission is known to be variable in time and shape (Turner et al. 1985), thus allowing for tests of different X- and  $\gamma$ -ray emission models.

To clarify the mechanism responsible for the X-ray emission, high quality data are first necessary to disentangle the contributions from the different spectral components, namely the jet and Seyfert components.

In this paper, we report on observations with *ASCA* during the first year of the mission. The source spectral properties are shown with particular attention to calibration uncertainties, most relevant in this source because it was used for on-board calibration of the CCDs. We show evidence of complex spectral features (soft-excess, Fe K emission line, flux and spectral correlated variability) and discuss their possible interpretation. Throughout the analysis we use  $H_0 = 50 \text{ km s}^{-1} \text{ Mpc}^{-1}$  and  $q_0 = 0$ .

## 2. Observations and Data Reduction

Over the period from 1993 June to 1993 December, 3C 273 was observed 9 times with the gas imaging spectrometer (GIS) and solid-state spectrometer (SIS) on-board the *ASCA* satellite (Tanaka, Inoue & Holt 1994). The observation log is given in Table 1. The SIS was operating in 1 CCD Faint mode during all the observations. Observations 2, 3, 5 and 6 have been used to calibrate each chip of the SIS (Dotani et al. 1996) and the remaining pointings are part of a multi-wavelength campaign on 3C 273 (von Montigny et al., 1997). Dark frame error (DFE) and echo corrections (Otani & Dotani 1994) have been applied to all the data. After removing hot and flickering pixels, standard selection criteria were used to select good observational intervals. The most relevant were an elevation and bright Earth angles greater than  $5^\circ$  and  $25^\circ$  respectively, and a magnetic cutoff rigidity greater than 8 GeV/c for SIS and 7 GeV/c for GIS. For all observations, source counts were extracted using circular region centered on the source of radius  $6'$  for the GIS and  $3'$  for the SIS. Hard X-ray emission was detected with *SIGMA* from a location about  $15'$  away from 3C 273 (at R.A.[1950]= $12^h27^m20^s$ , DEC[1950]= $02^\circ30'$  with an associated error of  $\sim 5'$ ) (Jourdain et al. 1992). We find no trace of such source in the *ASCA* field of views. Background spectra were obtained from the edges of the chips in the SIS and from the blank sky files in the GIS. The GIS background region was always chosen in regions uncontaminated by NGC 6552 and at similar off-axis distance as the source region (see Appendix A of Cappi et al. 1997 for a detailed discussion). Owing to the high count-rate of this bright source and the fact that the background typically contributed less than a few percent to the average count-rates in each observations, different choices of backgrounds (e.g. blank sky backgrounds for SIS or local backgrounds for GIS) did not introduce significant differences in the spectral results reported below. In total, *ASCA* collected about half a million counts per detector for an effective exposure time of  $\sim 160$  Ks for GIS and  $\sim 130$  Ks for SIS. Data preparation and spectral analysis have been done using version 1.2 of the XSELECT package and version 9.0 of the XSPEC program (Arnaud et al 1991). Official EA/PSF-V1.0 files, gis[23]v4.0.rmf and rsp1.1alphaPI1.6 matrices (released in 1994) were used for all the observations reported in the following. Newer XRT calibration files (EA/PSF-V2.0) and related GIS and SIS responses were also used in §3.4 for the study of the iron line emission.

## 3. Results

GIS2/3 and SIS0/1 pulse-height spectra were binned so as to have at least 200 counts per bin, in the energy ranges 0.7-10 keV and 0.4-10 keV, respectively. Light curves were accumulated for all observing periods, but none of these indicated significant variability (although variations as high as  $\sim 10$ -20% per observation period cannot be excluded). All photons were, thus, accumulated

observation-by-observation for the spectral analysis. It is emphasized that 3C 273 was used to calibrate the SIS response function imposing consistency with the GIS results (GIS was assumed to be well calibrated by fitting the Crab data with a single absorbed power law model; see Dotani et al. 1996 for details). Therefore, great care must be taken when interpreting the SIS results since systematic effects could be present. As a rule, *absolute* values obtained from the SIS (only) could not, in principle, be trusted. However, *relative* measurements (like flux and/or spectral variability) obtained from comparing different observations are likely to give valuable information since, in this case, systematic effects should cancel each other. Moreover, all the observations were taken during the first year of the mission, and the last 8 observations were performed within a period of 12 days. Thus, we assumed that the instrument did not change significantly from one observation to the other.

### 3.1. Flux Variability

First, GIS and SIS data were fitted separately with a single absorbed power law model, with the column density,  $N_{\text{H}}$ , free to vary. Throughout the analysis, the column density is calculated in the observer frame (i.e.  $z=0$ ). This model gives an acceptable description of all the spectra. The best-fitting model results are given in Table 2. It is emphasized that the 2-10 keV flux measurements (column 4 in Table 2) do not vary significantly even if  $N_{\text{H}}$  is fixed at the Galactic value (§3.3) or if an iron emission line is added to the model (§3.4). Figure 1 clearly shows that the flux varied in time by up to  $\sim 60\%$  on a time-scale of  $\sim 200$  days. Significant (20–30%) shorter-term variations on a time-scale of  $\sim 1$  day are also evident in the light-curve. The luminosity varied, accordingly, from  $L_{(2-10\text{keV})} \sim 1.4 \times 10^{46}$  erg s $^{-1}$  in observation 1 to a  $L_{(2-10\text{keV})} \sim 2.1 \times 10^{46}$  erg s $^{-1}$  in observation 9. Note that the photon indices obtained from the GIS and SIS are in excellent agreement, while there are slight, but significant, discrepancies in the measurement of the low energy absorption column. This effect will be considered in more detail in the following section. The 2–10 keV flux measured with the SIS is also systematically  $\sim 15\text{--}20\%$  higher than that obtained from the GIS. The discrepancy is currently attributed to cross calibration uncertainties that have been largely reduced to less than 10% with the introduction of new (EA/PSF-V2.0) XRT calibration files. With the matrices used in the present analysis, the SIS flux can be considered to be the most reliable with an absolute uncertainty of less than  $\sim 10\%$  (K. Arnaud et al., *ASCA* calibration uncertainties, [http://heasarc.gsfc.nasa.gov/docs/asca/cal\\_probs.html](http://heasarc.gsfc.nasa.gov/docs/asca/cal_probs.html)).

The absolute value and long time-scale variations of the 2-10 keV flux of 3C 273 are roughly consistent with previous observations with *EXOSAT* and *Ginga* satellites (Turner et al. 1990). However, the better quality and temporal sampling of the present observations also reveal for the

first time day-to-day variations of the 2–10 keV X-ray flux as large as  $\sim 20\%$ .

### 3.2. Soft Excess and Excess Absorption

90% confidence contours for the column densities versus photon indices obtained from the SIS spectra with the above absorbed power law model (Table 2) are shown in Fig. 2. The vertical lines represent the Galactic absorption (full line) and associated estimated errors (dotted lines) as obtained from measurements at 21 cm (Dickey & Lockman 1990). Fig. 2 clearly illustrates three interesting results: (1) The best-fit column density was significantly lower than the Galactic value during the first observation. This result can be promptly interpreted as evidence for a soft-excess in the data; (2) in all other observations, absorption was significantly, and systematically, higher than the Galactic value; (3) small, but significant, variations in the photon index are measured from observation to observation.

Note that, though the GIS is less sensitive than the SIS at low energies, the soft-excess is also detected in the GIS data. Indeed, the GIS spectrum gives an upper limit for  $N_{\text{H}}$  of  $\sim 0.65 \times 10^{20} \text{ cm}^{-2}$  during the first observation (significantly lower than  $N_{\text{Hgal}} \sim 1.79 \times 10^{20} \text{ cm}^{-2}$ ) while all other observations give  $N_{\text{H}}$  values consistent with the Galactic absorption. Although this measurement is in agreement with that reported by Yaqoob et al. (1994), these authors did not report the detection of a soft-excess for this observation probably because, in their work, SIS spectra were consistent with the Galactic absorption. This discrepancy is likely to be attributed to the fact that Yaqoob et al. (1994) used older response matrices obtained from the preliminary calibrations of the GIS and SIS instruments.

The evidence for a soft-excess during observation 1 is further strengthened by the ratio of the pulse height spectra of observation 1 divided by observation 9 of the summed SIS0 and SIS1 spectra (upper panel) and the summed GIS2 and GIS3 spectra (lower panel) shown in Fig. 3. Similar results were obtained dividing observation 1 with the other observations, thus excluding the possibility that the steepening of the ratios below about 2 keV could be due to a slight increase of the absorption measured during observation 9. Since pulse height spectral ratios directly compare the raw count-rates from two datasets, problems related to the calibration uncertainties of the instrumental response are in principle removed. These further confirm the presence of a continuum soft-excess emission at energies below  $\sim 1.5$  keV. In order to parameterize the measured soft-excess, two-component emission models were fitted to the GIS and SIS data of observation 1 with the absorption fixed at the Galactic value. Normalizations from the two detectors were free to vary independently. Results from the model-fittings are given in Table 3. Attempts to model the soft-excess with a Raymond & Smith (1977) plasma model and a warm absorber model, as proposed

in previous work, are not reported here since both models gave poor fits to the data, consistent with the absence of any blend of emission lines around 0.8–0.9 keV (quasar frame) or absorption features around 0.7–1.0 keV (quasar frame). Acceptable fits (Table 3) were obtained from either a black-body (with  $kT \sim 100$  eV) plus power law model, a bremsstrahlung (with  $kT \sim 240$  eV) plus power law model or a double power law model (with  $\Gamma_{\text{soft}} \sim 3$ ).

It is interesting to note that the improvement in  $\chi^2$  obtained with a double power law model is statistically significant when compared to the black-body ( $\Delta\chi^2 = 10$ ) or bremsstrahlung ( $\Delta\chi^2 = 5$ ) models at  $\sim 99.8\%$  and  $\sim 96\%$  confidence levels, respectively. This is similar to the findings of Leach et al. (1995) obtained from high quality *ROSAT* PSPC data and confirm that the soft-excess is better modeled by a power law than by a thermal emission model. This issue will be further addressed in §4.2. Moreover, it is likely that this soft-excess is intrinsically variable with time (in shape or in intensity) because our simulations indicate that, if constant, it should have been detected at least during observation 7, when the source was only  $\sim 15\%$  brighter than in observation 1.

The following 4 calibration observations and 4 AO-I observations are, instead, all consistent with a constant absorption column of  $\sim 3\text{--}4 \times 10^{20} \text{ cm}^{-2}$ . This value is significantly higher than the Galactic absorption by  $\sim 2\text{--}3 \times 10^{20} \text{ cm}^{-2}$ . However, a physical interpretation of this result cannot be made because the SIS responses were calibrated from some of these observations (Table 1) assuming that 3C 273 was absorbed by the Galactic column only. Instead, this column should, by definition, be taken as a systematic error of the *ASCA* SIS response function for a standard analysis like the one presented in this work. Similar results have been reported from independent work on 3C 273 (Hayashida et al. 1995) and the Coma cluster (Dotani et al. 1996; Hashimoto-dani, private communication).

### 3.3. Photon Index Variations

Figure 2 also suggests small but significant variations of the power law photon index, at least from observation 2 to observation 9. However, because of the presence of the soft-excess and extra-absorption mentioned above, these variations may be due to an incorrect modeling of the low energy absorption. To avoid such complications, only the data above 2 keV were considered. Since the photon indices obtained by separately fitting the GIS and SIS data were all consistent at  $\sim 90\%$  confidence level, the data from the two instruments were fitted simultaneously tying the fitting parameters together but allowing the relative normalizations to be free. A single power law model plus absorption fixed at the Galactic value was used in all fits. It is pointed out that since the SIS best-fit spectra normally require a value of  $N_{\text{H}}$  systematically higher than the Galactic value when fitted between  $\sim 0.4\text{--}10$  keV (see §3.2), by fixing the absorption at the Galactic value, a systematic

error will be introduced on the *absolute* value of the SIS photon indices. However, this (small) effect will not affect the measurements of *relative* values presented below. GIS results are not affected by these uncertainties. Best-fitting results are given in Table 4. The variations of the 2–10 keV photon indices with the observed 2–10 keV fluxes are shown in Fig. 4 for the (a) GIS+SIS data (all observations) and (b) GIS+SIS data, excluding calibration observations n. 2, 3 and 5. The reason we ignored observations 2, 3 and 5 in the dataset (b) is that these were performed using chips 0, 2 and 3 of SIS0 and chips 0, 1, 2 of SIS1 in which the gain (relative to the standard chip n.1 of SIS0 and chip n. 3 of SIS1) are uncertain by as much as  $\sim 2\%$  (Dotani et al. 1996). This could introduce systematic errors in the spectral slope of as much as  $\sim 0.05$  which are much larger than our statistical errors and could, therefore, distort any significant statistical correlation.

Figure 4 shows evidence for a spectral index change in 3C 273. Though the variations are not large ( $\Delta\Gamma \lesssim 0.1$ ), they are significant in both datasets (Table 5). This point is further illustrated in Figure 3 which shows that, though the data are somewhat noisy above  $\sim 8$  keV, the pulse height spectrum between 2–10 keV of observation 1 is steeper than that of observation 9, for both the GIS and SIS data. Table 5 shows the results from  $\chi^2$ -tests against constancy, linear correlation coefficients and rank correlation coefficients for the two datasets considered. The most interesting result obtained from this analysis is that there is a trend (most noticeable in Fig. 4) for the 2–10 keV photon index to be anti-correlated with the flux, i.e. a spectral flattening as the source brightens. This result is significant at a  $\sim 99.95\%$  and  $\sim 81\%$  confidence level for the dataset (a) and at a  $\sim 99.999\%$  and  $\sim 89\%$  confidence level for dataset (b), for a linear and non-parametric correlation respectively (Table 5). It is emphasized that the same trend was observed also in both SIS and GIS instruments taken individually, though with somewhat lower significance. However, it should be noted that the significance of this result depends mostly on the 2 data points from observations 1 and 9. If real, this behavior is opposite to that commonly seen in Seyfert galaxies (e.g. Mushotzky, Done & Pounds 1993 and references therein) and, on the contrary, provides an interesting analogy with BL Lac objects as discussed in §4.

### 3.4. Iron Emission Line

The spectra have been inspected for the presence of an iron emission line. Our first analysis clearly reveals the presence of a broad ( $\sigma \sim 0.4$  keV) Fe K line with EW  $\sim 90$ – $100$  eV during observations 1 and 7 (Table 6). Confidence contours in the Fe K parameters space  $\sigma$ –E and EW–E (observer frame) obtained from fitting the observation 1 data are shown in Fig. 5 as an example. A narrow line is also significant in 4 out of 7 of the remaining observations. The emission lines are all consistent with a neutral or mildly ionized iron emission line (at 6.4 keV in the quasar’s frame) at



$\sim 90\%$  confidence level. We find no significant correlation between the equivalent width of the Fe K line and the computed X-ray flux but it is interesting that the 2 strongest lines are detected while 3C 273 was in its lowest states (i.e. observations 1 and 7 reported in Table 6).

However, as is evident from the dashed contours shown in Fig. 5, the GIS spectra of the Crab which were used to calibrate the GIS exhibit a miscalibration at similar energies which can be modeled with a broad ( $\sigma \simeq 0.4 \pm 0.05$  keV) line at  $E \simeq 5.7 \pm 0.05$  keV with an EW  $\simeq 50 \pm 15$  eV (see also Ebisawa et al. 1996 for more details about this miscalibration in the Crab's GIS spectra).

New calibration matrices (ascaarf v2.62 with version 2.0 of the XRT matrices) have, however, recently been distributed to the *ASCA* guest observers through the *ASCA* Goddard Guest Observer Facility (K. Ebisawa, [http://heasarc.gsfc.nasa.gov/docs/asca/xrt\\_new\\_response\\_announce/announce.html](http://heasarc.gsfc.nasa.gov/docs/asca/xrt_new_response_announce/announce.html)). The new calibrations reduce the systematic differences in flux between GIS and SIS (see §3.1) and corrects the GIS and SIS response matrices for the  $\sim 5$ –6 keV spectral feature detected in the Crab spectra (Fukazawa, Ishida & Ebisawa 1997, but see also Gendreau & Yaqoob 1997). It is emphasized that the use of this improved calibration does not affect our conclusions on flux variability, soft-excess and spectral variability because, as stated in §3, only relative measurements have been considered. It gives, however, significantly different results on the iron emission line measurements. Now, spectral fitting yields narrow ( $\sigma < 0.21$  keV and  $< 0.6$  keV) and weaker, EW ( $\sim 25$  eV and 27 eV, observer frame) lines during observations 1 and 7, respectively (see Table 7). The line is also reduced in all other observations yielding only upper limits ranging between  $\sim 10$ –30 eV. Analysis with the latest available calibration suggests, therefore, that the line detected during observations 1 and 7 is very likely to be real but that, contrary to our first results with previous calibration, it is consistent with being narrow and with having an EW  $\sim 20$ –30 eV (observer frame). In the quasar's frame, the Fe K line best-fit parameters are  $E \simeq 6.47^{+0.09}_{-0.07}$  keV,  $6.31^{+0.06}_{-0.06}$  keV and  $EW \simeq 29^{+23}_{-15}$  eV,  $31^{+18}_{-18}$  eV for observations 1 and 7, respectively. These results agree with the emission of a fluorescent narrow Fe  $K_{\alpha}$  line from neutral matter (Makishima 1986).

## 4. Discussion

### 4.1. On the X-ray Continuum Emission: Signatures of a Jet Component ?

The *ASCA* observations have shown that the 2–10 keV flux is variable with time by up to  $\sim 60\%$  on a time-scale of  $\sim 200$  days and shows day-to-day variations as large as  $\sim 20\%$ . Thus, unless it is relativistically beamed, the hard X-ray source must be smaller than  $R = c \times \Delta t \sim 10^{16}$  cm where the source doubling time-scale, i.e. the time necessary for the source to vary by a factor of two, can

roughly be estimated as  $\Delta t \sim \frac{E_{\text{init}}}{\Delta F} \times \frac{\Delta t_{\text{obs}}}{1+z}$ , where  $z$  is the source redshift. It is well known that 3C 273 shows a one-sided jet which is clearly observed at both radio and optical wavelengths (Bahcall et al. 1995 and references therein) which is most likely produced by synchrotron emission from relativistic electrons (3C 273 exhibits superluminal motion with  $\beta_{\text{app}} \simeq 8.0 \pm 1.0$ , e.g. Vermeulen & Cohen 1994). The main jet consists of a number of bright, elongated, knots extending from  $\sim 30$  kpc to  $\sim 50$  kpc from the quasar with kpc-scale transverse dimensions in both the radio and optical images. Therefore, the dimensions of the radio-optical jet are about 6 orders of magnitude larger than the X-ray source dimension. This, together with the high X-ray luminosity of  $\sim 1.5\text{-}2 \times 10^{46}$  erg s $^{-1}$  inferred from the X-ray data, excludes the possibility that the bulk of the X-ray emission is produced by the jet’s knots only (whatever the emission mechanism is). Therefore, if it is related to the jet, the 2-10 keV X-ray emitting region must be located in the innermost regions of the jet. These conclusions are consistent with high resolution X-ray imaging (e.g. *ROSAT* HRI) of the jet emission of 3C 273 (Röser et al. 1996).

For the first time in this source, we find evidence for a statistically significant anti-correlation between the 2-10 keV flux and spectral index, implying hardening of the spectrum as the source brightens. This is opposite to lower luminosity AGNs (e.g. Seyfert 1 galaxies) which often show a positive correlation (Grandi et al. 1992, Mushotzky, Done & Pounds 1993, and references therein) but similar to the anti-correlation flux-spectral index often observed in BL Lacertae objects (at least in X-ray selected BL Lac objects; e.g. Giommi et al. 1990, Urry et al. 1996). This suggests that the bulk of the X-ray emission in 3C 273 is produced by a mechanism similar to the one supposed in BL Lac objects, i.e. a process related to the existence of a beam of relativistic particles (e.g. Fichtel 1995). This is consistent with the recent results of von Montigny et al. (1997) which show that the multi-wavelength spectrum (from radio to  $\gamma$ -rays) of 3C 273 can be explained by any of the most prominent theoretical models (e.g. synchrotron self-Compton (SSC, Maraschi, Ghisellini & Celotti 1992), inverse Compton on external photons from an accretion disk or a broad-line region (EC, Sikora, Begelman & Rees 1994) or synchrotron from ultra-relativistic electrons and positrons in a proton-induced cascade (Mannheim & Biermann 1992)) for the explanation of the high  $\gamma$ -ray emission of BL Lac objects. On the basis of the present *ASCA* data, it is not possible, however, to distinguish between the different theoretical models since all of these could explain the observed spectral variability. Synchrotron losses, for example, have often been invoked to explain a steepening with decreasing flux (e.g. in PKS 2155-304, Sembay et al. 1993; in H0323+022, Kohmura et al. 1994; in Mkn 421, Takahashi et al. 1996). In these cases, the X-ray spectra were interpreted as the high energy tail of synchrotron emission, while the X-ray spectrum of 3C 273 is more likely due to Compton emission (von Montigny et al. 1997). However, one could expect that a similar behavior may hold also in the “Compton” bump, though perhaps at a different time-scale because of a possibly different emission region. Moreover, hysteresis “clockwise” flux-index relations were

reported in these BL Lac objects. Further observations are clearly necessary to test this hypothesis in 3C 273.

Alternatively, there might be a mixture of, say, SSC and EC contributing to the X-ray emission, the spectrum being harder when the EC flux increases. Or else, as discussed next, there might be a contribution from a Seyfert-like spectrum with a steeper spectral slope, e.g.  $\Gamma \sim 1.7$  as commonly seen in Seyfert galaxies (Mushotzky, Done & Pounds 1993), which steepens the spectrum as the source becomes fainter. A small contribution of  $\sim 10\text{-}20\%$  in the 2-10 keV band could steepen the observed spectrum by  $\Delta\Gamma \sim 0.1$  thus explain the flux-index anti-correlation.

#### 4.2. On the X-ray Spectral Features: Signatures of a Seyfert-like Component ?

Another interesting result from our analysis is that the spectra intermittently show clear evidence for a separate soft component below  $\sim 2$  keV. This component was observed only during the first observation, when the source was faintest. The best fit values for this component (see §3.2) are in good agreement with previous *EXOSAT*, *EINSTEIN*, *GINGA* and *ROSAT* findings (e.g. Courvoisier et al. 1987, Wilkes & Elvis 1987, Turner et al. 1990, Staubert 1992, Leach et al. 1995), in particular if one allows for cross-calibration uncertainties and considers that previous observations usually found, or fixed, the photon index between 2-10 keV at a slightly flatter value of  $\Gamma \sim 1.5$  than found with *ASCA*. The issue of interpreting the soft continuum cannot, however, be addressed in more detail with the present *ASCA* data since, as explained in §3, absolute values obtained from the SIS cannot in principle be trusted because 3C 273 was used to calibrate the SIS response (see Dotani et al. 1996 for details on the calibration procedure). For example, because of the systematic excess absorption found in §3.2 which is most likely attributed to a calibration uncertainty, we cannot trust absolute values of the best-fit parameters for the soft-excess. Only relative measurements can be considered, which tell us that a soft excess component is indeed required by the data during observation 1 and not during the following observations.

It should be pointed out, however, that as found by Leach et al. (1995) from the *ROSAT* PSPC data, the soft component is modeled better by a single power law with absorption at the Galactic value ( $\Delta\chi^2 = 10$  and 5 compared to the black-body and bremsstrahlung models, respectively). This may indicate that the data are not well described by a model with a concave shape but rather prefer a straight or convex model. At this point, it is interesting to note that a recent *Beppo-SAX* observation of 3C 273 performed in July 1996, when the source was at very low flux level ( $\sim 7.1 \times 10^{-11}$  erg cm $^{-2}$  s $^{-1}$ ), shows evidence for both a soft excess emission (below  $\sim 0.3$  keV) and a strong absorption structure at  $\sim 0.5$  keV indicating, possibly, the presence of a warm absorber in 3C 273 (Grandi et al. 1997). *ASCA* observed 3C 273 simultaneously with *Beppo-SAX* on that occasion.

Results of this observation will be presented elsewhere (Yaqoob et al., in preparation). Fitting the *ASCA* observation 1 with a warm absorber model only does not however improve the spectral fitting significantly since, clearly, the data require some extra emission below  $\sim 2$  keV that cannot be explained with absorption features alone. Addition of an absorption edge at  $\sim 0.5$  keV to the double power model increases the quality of the fit slightly but not significantly.

The *ASCA* spectra also reveal evidence for iron line emission in 3C 273 on two different occasions, during observations 1 and 7, when the source was faintest. The best-fit parameters of the Fe K line obtained from the fitting of the SIS data only with the latest available response matrices are consistent with the line being narrow and weak (EW  $\sim 20$ -30 eV in both observations 1 and 7). These values are in reasonable agreement with the *GINGA* results of Turner et al. (1990) and the *Beppo-SAX* results of Grandi et al. (1997), who both found a significant iron line in 3C 273 when the source was in a low ( $F_{(2-10\text{keV})} \lesssim 1 \times 10^{-10}$  erg cm $^{-2}$  s $^{-1}$ ) state, similar to the results reported here. The line emission and, also the soft excess emission suggest that, at least during observations 1 and 7, a Seyfert-like component underlying a dominant simple power-law (jet ?) component contributes significantly to the X-ray spectrum of 3C 273. In order to give a rough quantitative estimate of the contribution from the Seyfert and to test this overall picture, we tried to fit the broad-band ( $\sim 0.4$ -300 keV) *ASCA* plus *OSSE* spectrum with a model consisting in the sum of: a power-law with  $\Gamma \simeq 1.5$ -1.6, a ‘‘typical’’ Seyfert-like spectrum (Nandra & Pounds 1994), i.e. a power-law (with  $\Gamma=1.9$ ) plus a reflection component (with  $R = \frac{\text{normalization of the reflected component}}{\text{normalization of the direct component}} = 1$  corresponding to a  $2\pi$  coverage of the reflector) and associated iron line (with an equivalent width fixed at 150 eV, with respect to the Seyfert continuum, e.g. George & Fabian 1991), and a black-body. The *ASCA* spectra are from observation 1 and the *OSSE* spectrum is from the observation performed during 1991 June 15-28 (viewing period n.3 reported in Johnson et al. 1995). As demonstrated by the unfolded spectrum and residuals shown in Fig. 6, an acceptable fit is obtained with a black-body temperature of  $kT \sim 100$  eV, slightly reduced compared to the results given in Table 3 because of the Seyfert power law contribution, and with the Seyfert-like spectrum contributing about 30% at 1 keV and about 10-20% in the 2-10 keV energy band to the total spectrum. However, it is stressed that while the present data are consistent with this picture, there is actually no direct evidence for a steep ‘‘Seyfert-like’’ power-law, since its contribution cannot be unambiguously disentangled from the softer black-body component. However, we have also shown in §3.2 that the soft-excess emission is likely to be variable in time and, as discussed above, is better fitted with a model with a convex shape rather than a concave one. These may be the indication that some direct, steep, Seyfert-like component contributes partly to the soft-excess emission of 3C 273.

An alternative explanation for the Fe K line emission may be reflection off optically thick matter (e.g. broad-line region blobs and/or a molecular torus and/or an accretion disk, located

near the jet region) from the jet continuum itself. In such case, the estimation of the expected iron line intensity is complicated by the possibility that the X-ray and hard X-ray radiation could be beamed in the direction of, or away from, the reflecting matter and its precise evaluation is beyond the scope of this paper. The effect of the unknown effective covering factor of the reflector should also be taken into account.

## 5. Conclusions

To date, *ASCA* has observed 3C 273 10 times. Results from the first 9 observations, all performed during the first year of the mission have been presented here. These confirm and expand the evidence that the X-ray emission of 3C 273 is complex, with different spectral components contributing to its X-ray emission. Because 4 of the 9 observations were used for the on-board calibration of the CCDs, great care had to be taken when interpreting the observational results for this source. As a rule, *absolute* values, in particular those obtained from the SIS, require a detailed estimate and knowledge of the instrumental systematic errors to be trusted. *Relative* measurements (like flux and/or spectral variability) obtained from comparing different observations are, however, more reliable since they should not be affected by calibration uncertainties.

With this caveat in mind, it is found that:

1. A conservative systematic error at low energies that corresponds to an extra-absorption column of  $\sim 2\text{--}3 \times 10^{20} \text{ cm}^{-2}$  is found for the SIS response, consistent with the *ASCA* Team's official prescriptions.
2. 2–10 keV flux variations by up to  $\sim 60\%$  on a time-scale of  $\sim 200$  days and day-to-day variations as large as  $\sim 20\%$  were observed.
3. Extra soft X-ray emission is required by the data during the first observation, when the source was in its lowest flux level.
4. Flux and spectral slope variations are clearly detected as well and, for the first time, there is a statistically significant evidence that the index and flux are anti-correlated.
5. Iron line emission is detected in (only) the two observations with the lowest flux levels. The line is in both cases weak ( $EW \sim 20\text{--}30 \text{ eV}$ ), but statistically significant at more than 99% confidence level, narrow and consistent with Fe  $K_{\alpha}$  emission from neutral matter.

We then speculate that all the above observable properties of the X-ray spectrum of 3C 273 can be interpreted in terms of the sum of two emission mechanisms. These are a non-thermal emission

from the innermost regions of the jet which dominates the 2-10 keV region and whose signatures are the spectral variability and a flat ( $\Gamma \sim 1.6$ ) power law continuum (that extrapolates well into higher energies), plus a diluted Seyfert-like spectrum whose signatures are the soft-excess and iron line emission. The newly discovered index-flux anti-correlation may be interpreted either by intrinsic variations of the jet power law index or by some contribution of the Seyfert-like continuum spectrum (say, a power law with  $\Gamma \sim 1.9$ ) as the jet component varies. The overall scenario predicts that when the (dominant) jet component is in a low flux state, the spectral features produced by the Seyfert-like spectrum should be more easily detected (owing for variability of the Seyfert-like spectrum itself).

### ACKNOWLEDGEMENTS

We are grateful to the *ASCA* team in ISAS for their operation of the satellite and to the *ASCA* GOF at NASA/GSFC for their assistance in data analysis. M.C. acknowledges colleagues in the Institute of Physical and Chemical Research (RIKEN) for their warm hospitality and the Italian Space Agency (ASI) for financial support. C.O. acknowledges the Special Postdoctoral Researchers Program of RIKEN for support. KML gratefully acknowledges support through NAG5-3307 (*ASCA*). We thank T. Yaqoob, T. Dotani, K. Gendreau and T. Kotani for very helpful discussion on the calibration-related issues and H. Kubo and G. Ghisellini for usefull comments.

## REFERENCES

- Arnaud, K.A., Haberl, F., & Tennant, A., 1991, XSPEC User's Guide, ESA TM-09
- Bahcall, J.N., Kirhakos, S., Schneider, D.P., Davis, R.J., Muxlow, T.W.B., Garrington, S.T., Conway, R.G., & Unwin, S.C., 1995, ApJL, 452, 91
- Cappi, M., Matsuoka, M., Comastri, A., Brinkmann, W., Elvis, E., Palumbo, G.G.C., & Vignali, C., 1997, ApJ, 478, 492
- Courvoisier, T.J.L., et al., 1987, A&A, 176, 197
- Dickey, J.M. & Lockman, F.J., 1990, ARA&A, 28, 215
- Dondi, L. & Ghisellini, G., 1995, MNRAS, 273, 583
- Dotani, T., et al., 1996, ASCA News n. 4, 3
- Ebisawa, K., Ueda, Y., Inoue, H., Tanaka, Y., & White, N.E., 1996, ApJ, 467, 419
- Elvis, M., et al., 1994, ApJS, 95, 1
- Fichtel, C.E., 1994, ApJS, 90, 917
- Fukazawa, Y., Ishida, M. & Ebisawa, K, 1997, ASCA News n. 5, 3
- Gendreau, K., & Yaqoob, T., 1996, ASCA News n. 5, 8
- George, I.M., & Fabian, A.C., 1991, MNRAS, 249, 352
- Giommi, P., Barr, P., Pollock, A.M.T., Garilli, B., & Maccagni, D., 1990, ApJ, 356, 432
- Grandi, P., Sambruna R.M., Maraschi L., Matt G., Urry M., Mushotzky R.F., 1997, ApJ, 487, 636
- Hayashida, K., Miura, N., Hashimoto-dani, K., & Murakami, S., 1995, ISAS Internal Report
- Johnson W.N., et al., 1995, ApJ, 445, 182
- Jourdain, E., et al., 1992, ApJL, 395, 69
- Kohmura, Y., Makishima, K., Tashiro, M., Ohashi, T. & Urry, C.M., 1994, PASJ, 46, 131
- Leach, C.M., Mc Hardy, I.M., & Papadakis, I.E., 1995, MNRAS, 272, 221
- Lichti, G.G., et al., 1995, A&A, 298, 711
- Makishima, K., 1986, in Lectures Notes in Physics, Vol. 266, The physics of Accretion onto Compact Objects, ed. K.O. Mason, M.G. Watson & N.E. White (Berlin:Springer), 249
- Mannheim, K., & Biermann, P.L., 1992, A&A, 253, L21
- Maraschi, L., Ghisellini, G., & Celotti, A., 1992, ApJ, 397, L5
- Mushotzky, R.F., Done, C., & Pounds, K.A., 1993, ARA&A, 31, 717
- Nandra, K., & Pounds, K.A., 1994, MNRAS, 268, 405
- Otani, C., & Dotani, T., 1994, ASCA News n. 2, 25

- Raymond, J.C., & Smith, B.W., 1977, *ApJS*, 35, 419
- Röser, H.-J., Meisenheimer, K., Neumann, M., & Conway, R.G., 1996, in *Proc. Röntgenstrahlung from the Universe*, Würzburg, Germany, Ed. H.-U. Zimmermann, J.E. Trümper & H. Yorke, MPE Report 263, 499.
- Sambruna, R.M., Maraschi, L., & Urry, C.M., 1996, *ApJ*, 463, 444
- Sembay, S., Warwick, R.S., Urry, C.M., Sokoloski, J., George, I.M., Makino, I.M., Ohashi, F., & Tashiro, M., 1993, *ApJ*, 404, 112
- Sikora, M., Begelman, M.C. & Rees, M., 1994, *ApJ*, 421, 153
- Staubert, J., 1992, in “X-ray emission from Active Galactic Nuclei and the Cosmic X-ray Background”, Ed. W. Brinkmann & J. Trümper (MPE Report 235), p 42
- Takahashi, T., et al., 1996, *ApJL*, 470, 89
- Tanaka, Y., Inoue, H., & Holt, S.S., 1994, *PASJ*, 46, 37
- Turner, M.J.L., et al. 1990, *MNRAS*, 244, 310
- Urry, C.M., et al., 1996, *ApJ*, 463, 424
- Urry, C.M., & Padovani, P., 1995, *PASP*, 107, 803
- Vermeulen, R.C., & Cohen, M.H., 1994, *ApJ*, 430, 467
- von Montigny, C., et al., 1997, *ApJ*, 483, 161
- Walter, R., Orr, A., Courvoisier, T.J.L., Fink, H.H., Makino, F., Otani, C., & Wamsteker, W., 1994, *A&A*, 285, 119
- Wilkes, B.J., & Elvis, M., 1987, *ApJ*, 323, 243
- Yaqoob, T., et al. 1994, *PASJ*, 46, L49



Table 1: Observations log

Obs.	Start Time (UT)	Exposure* (s)		CR*(s <sup>-1</sup> )		SIS Mode	Comment
		GIS	SIS	GIS	SIS		
1	08/06/93 20:11	33300	24945	2.25	3.25	1CCD	PV (Yaqoob et al. 94)
2	15/12/93 12:34	18130	14207	2.85	4.10	1CCD	PV calib s0c2
3	15/12/93 23:53	21230	17033	3.88	4.96	1CCD	PV calib s0c0
4	16/12/93 12:11	13295	9488	3.67	4.44	1CCD	AOI
5	19/12/93 23:45	19867	16136	3.04	4.17	1CCD	PV calib s0c3
6	20/12/93 10:45	19390	15497	2.88	5.32	1CCD	PV calib s0c1
7	20/12/93 22:03	12291	10398	2.75	3.69	1CCD	AOI
8	23/12/93 23:35	11605	10325	2.84	3.72	1CCD	AOI
9	27/12/93 13:58	10493	7169	3.39	4.37	1CCD	AOI

\* Exposure and count-rates are average for GIS and SIS detectors.

Table 2: Results Using a Single Absorbed Power Law Model

Obs.	Instrument	$N_{\text{H}}^a$	$\Gamma$	$F_{\text{X}}^b(2-10 \text{ keV})$	$\chi_{\text{red}}^2/\text{d.o.f.}$
1	GIS	$< 0.65$	$1.63_{-0.01}^{+0.01}$	1.04	1.34/518
	SIS	$< 0.19$	$1.64_{-0.01}^{+0.01}$	1.23	1.62/350
2	GIS	$< 1.86$	$1.62_{-0.02}^{+0.02}$	1.33	1.04/412
	SIS	$4.31_{-0.59}^{+0.57}$	$1.60_{-0.02}^{+0.01}$	1.53	1.62/296
3	GIS	$< 1.80$	$1.60_{-0.02}^{+0.01}$	1.54	1.05/546
	SIS	$4.48_{-0.56}^{+0.52}$	$1.60_{-0.01}^{+0.02}$	1.70	1.73/358
4	GIS	$3.09_{-1.84}^{+1.83}$	$1.62_{-0.02}^{+0.03}$	1.56	0.95/382
	SIS	$4.18_{-0.68}^{+0.64}$	$1.59_{-0.02}^{+0.02}$	1.71	1.02/445
5	GIS	$< 1.50$	$1.53_{-0.01}^{+0.02}$	1.45	1.16/463
	SIS	$3.54_{-0.55}^{+0.54}$	$1.53_{-0.02}^{+0.02}$	1.58	1.94/319
6	GIS	$2.69_{-1.65}^{+1.73}$	$1.58_{-0.02}^{+0.02}$	1.31	1.105/443
	SIS	$3.67_{-0.59}^{+0.60}$	$1.56_{-0.02}^{+0.02}$	1.51	1.30/300
7	GIS	$< 2.44$	$1.59_{-0.02}^{+0.03}$	1.22	0.96/263
	SIS	$3.55_{-0.71}^{+0.68}$	$1.58_{-0.03}^{+0.02}$	1.44	1.22/430
8	GIS	$< 3.61$	$1.56_{-0.02}^{+0.03}$	1.30	1.09/259
	SIS	$3.89_{-0.71}^{+0.70}$	$1.55_{-0.02}^{+0.02}$	1.48	1.08/435
9	GIS	$3.57_{-2.10}^{+2.15}$	$1.54_{-0.02}^{+0.03}$	1.57	1.01/272
	SIS	$5.01_{-0.85}^{+0.83}$	$1.52_{-0.03}^{+0.02}$	1.82	1.04/391

<sup>a</sup> Absorption column density in units of  $10^{20} \text{ cm}^{-2}$ .

<sup>b</sup> Observed flux in units of  $10^{-10} \text{ erg cm}^{-2} \text{ s}^{-1}$ .

Note: Errors are 90 % confidence for 2 interesting parameters ( $\Delta\chi^2=4.61$ ).

Table 3: SIS – Two Component Models Fitted to the Observation 1 Data

	$kT/\Gamma_{\text{soft}}$ (eV)	$\Gamma/\Gamma_{\text{hard}}$	$L_X^a(0.1-2.0 \text{ keV})$ ( $10^{45} \text{ erg s}^{-1}$ )	$\chi_{\text{red}}^2/\text{d.o.f.}$
black body + power law	$119_{-16}^{+16}$	$1.64_{-0.02}^{+0.02}$	1.07	1.46/869
bremss. + power law	$281_{-70}^{+89}$	$1.64_{-1.62}^{+1.66}$	2.38	1.45/869
Two power laws	$2.99_{-0.85}^{+0.84}$	$1.59_{-0.09}^{+0.08}$	5.70	1.44/869

<sup>a</sup> calculated from only the soft component and the SIS normalization. Values with the GIS normalization were approximately 15% lower.

Note: Intervals are at 90 % confidence for 2 interesting parameters.

Table 4: Fits between 2-10 keV with a Single Absorbed Power Law Model -  $N_{\text{H}} \equiv N_{\text{Hgal}}$

Obs.	$\Gamma$	$F_X^a(2-10 \text{ keV})$	$\chi_{\text{red}}^2/\text{d.o.f.}$
1	$1.62_{-0.01}^{+0.01}$	1.22	1.50/454
2	$1.58_{-0.02}^{+0.02}$	1.48	1.47/334
3	$1.59_{-0.01}^{+0.01}$	1.67	1.40/498
4	$1.56_{-0.02}^{+0.02}$	1.69	1.05/434
5	$1.52_{-0.01}^{+0.01}$	1.56	1.22/403
6	$1.57_{-0.01}^{+0.01}$	1.49	1.15/371
7	$1.57_{-0.02}^{+0.02}$	1.41	1.24/370
8	$1.55_{-0.02}^{+0.02}$	1.47	1.02/378
9	$1.52_{-0.02}^{+0.02}$	1.77	1.06/355

<sup>a</sup> Observed SIS flux in units of  $10^{-10} \text{ erg cm}^{-2} \text{ s}^{-1}$ . GIS flux was typically  $\sim 15-20\%$  lower.

Note: Intervals are at 90 % confidence for 1 interesting parameter ( $\Delta\chi^2=2.71$ ).

Table 5:  $\Gamma_{2-10\text{keV}} - F_X(2-10 \text{ keV})$  correlations

Instrument	d.o.f.	$\chi^2$ , <sup>a</sup>	p <sup>a</sup>	r <sup>b</sup>	p <sup>b</sup>	r <sub>s</sub> <sup>c</sup>	p <sup>c</sup>
GIS+SIS (all)	9	35.1	$5.7 \times 10^{-5}$	-0.64	$\sim 0.05$	-0.48	0.19
GIS+SIS <sup>d</sup>	6	20.4	$2.3 \times 10^{-3}$	-0.89	$\sim 1 \times 10^{-3}$	-0.71	0.11

<sup>a</sup>  $\chi^2$  value and corresponding probability (p) for a  $\chi^2$  test against constancy.

<sup>b</sup> Linear correlation coefficient (r) and corresponding probability (p) for a linear correlation of the data.

<sup>c</sup> Spearman rank-order coefficient (r<sub>s</sub>) and corresponding probability (p) for a non-parametric correlation of the data.

<sup>d</sup> GIS plus SIS data excluding observations 2, 3 and 5 which were used to calibrate the “non-standard” SIS chips.

Table 6: Iron emission line best-fit parameters\*

	$\Gamma_{2-10\text{keV}}$	E (keV)	$\sigma$ (keV)	EW (eV)	$\chi^2_{red}/\text{d.o.f.}$
Old calibration software and matrices					
Obs. 1	$1.63^{+0.01}_{-0.01}$	$5.59^{+0.04}_{-0.04}$	0 (fixed)	$40^{+10}_{-15}$	1.44/454
	$1.63^{+0.01}_{-0.01}$	$5.67^{+0.10}_{-0.12}$	$0.43^{+0.23}_{-0.19}$	$100^{+48}_{-34}$	1.43/453
Obs. 7	$1.57^{+0.02}_{-0.02}$	$5.46^{+0.04}_{-0.04}$	0 (fixed)	$38^{+17}_{-17}$	1.21/372
	$1.57^{+0.02}_{-0.02}$	$5.44^{+0.16}_{-0.15}$	$0.28^{+0.25}_{-0.10}$	$81^{+29}_{-29}$	1.20/371
New calibration software and matrices					
Obs. 1	$1.56^{+0.01}_{-0.01}$	$5.59^{+0.08}_{-0.06}$	0 (fixed)	$25^{+20}_{-13}$	1.26/454
	$1.56^{+0.01}_{-0.01}$	$5.59^{+0.15}_{-0.10}$	< 0.21	$27^{+50}_{-12}$	1.26/453
Obs. 7	$1.52^{+0.04}_{-0.03}$	$5.45^{+0.05}_{-0.05}$	0 (fixed)	$27^{+16}_{-15}$	1.23/372
	$1.52^{+0.04}_{-0.04}$	$5.45^{+0.07}_{-0.06}$	< 0.59	$34^{+11}_{-24}$	1.23/371

\* The continuum emission was fitted between 2-10 keV with a single absorbed power law with  $N_H = N_{Hgal} = 1.79 \times 10^{20} \text{ cm}^{-2}$ .

Note: Intervals are at 90 % confidence for 1 interesting parameter ( $\Delta\chi^2=2.71$ ).

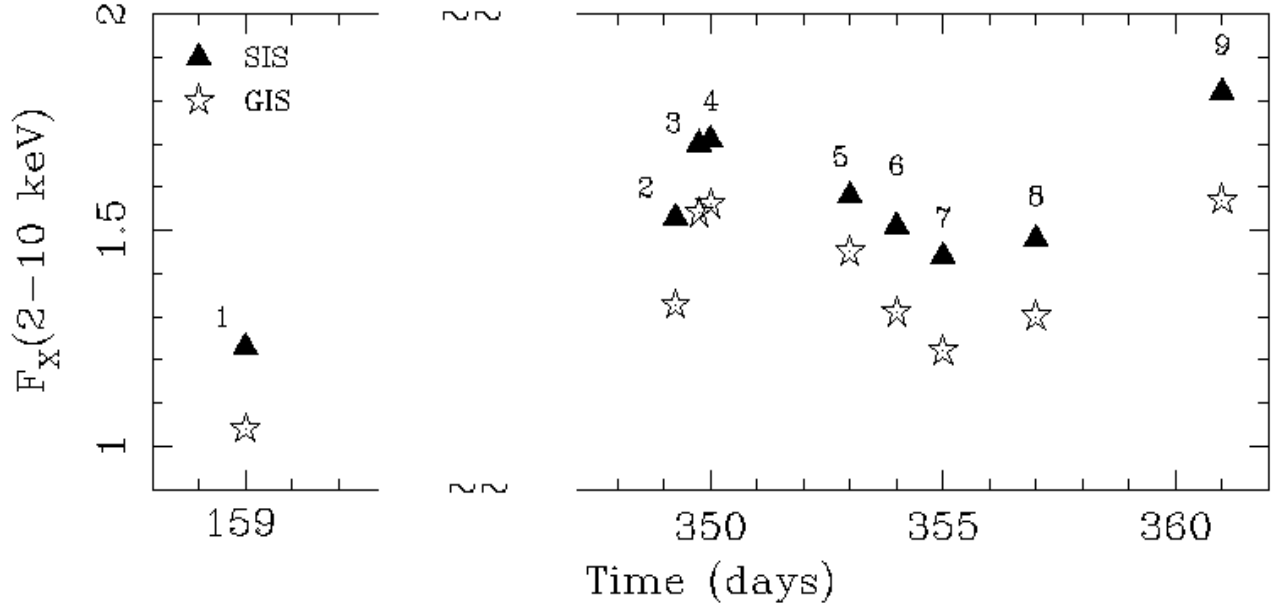


Fig. 1.— Variation with time (since the mission started) of the 2-10 keV flux. Note the temporal gap between the first and following observations. Fluxes are in units of  $10^{-10}$  erg  $\text{cm}^{-2}$   $\text{s}^{-1}$ . Flux statistical errors are estimated to be conservatively smaller than 10%.

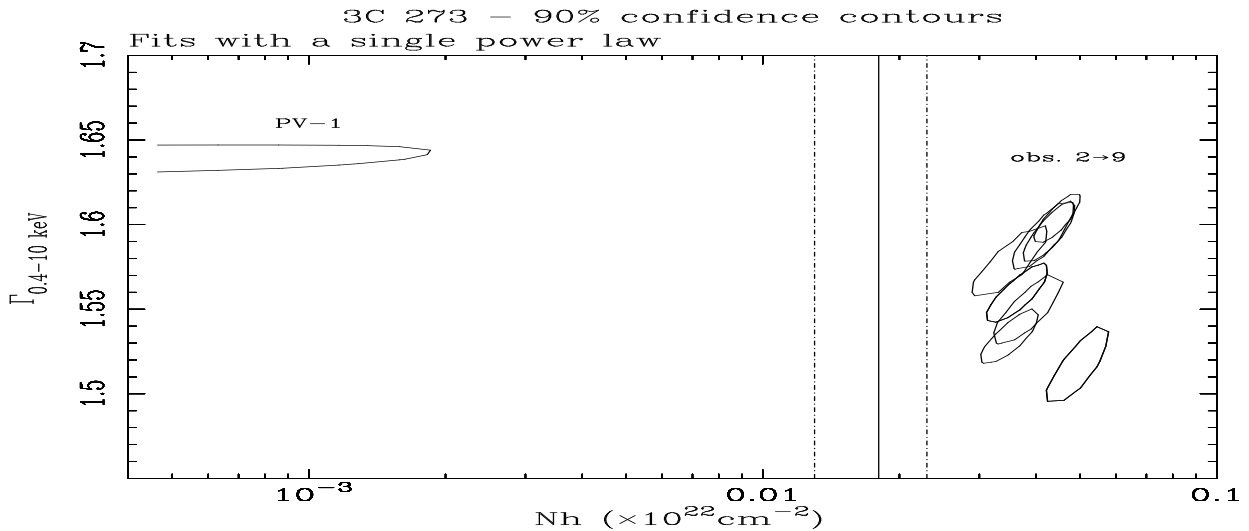


Fig. 2.— 90% confidence contours of absorption vs photon index obtained the SIS, for a single absorbed power law model, illustrating the soft-excess, extra absorption and spectral variability. The vertical line represents the Galactic absorption (full line) and associated errors (a conservative error of 30% as been assumed, Dickey & Lockman 1990).

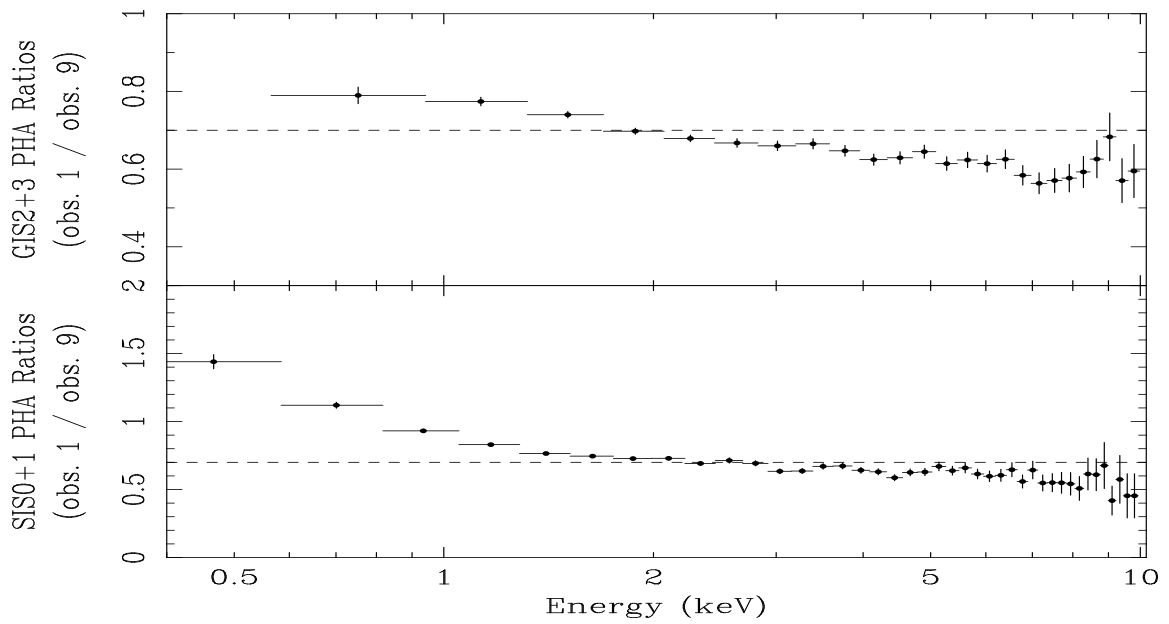


Fig. 3.— PHA ratios of observation 1 divided by observation 9 which illustrate the soft-excess during observation 1. The 2-10 keV spectrum during observation 1 appears to be steeper than during observation 9. An horizontal (dashed) line is plotted to better show the spectral variations. Note that the line-like feature present at  $\sim 8$  keV is not statistically significant.

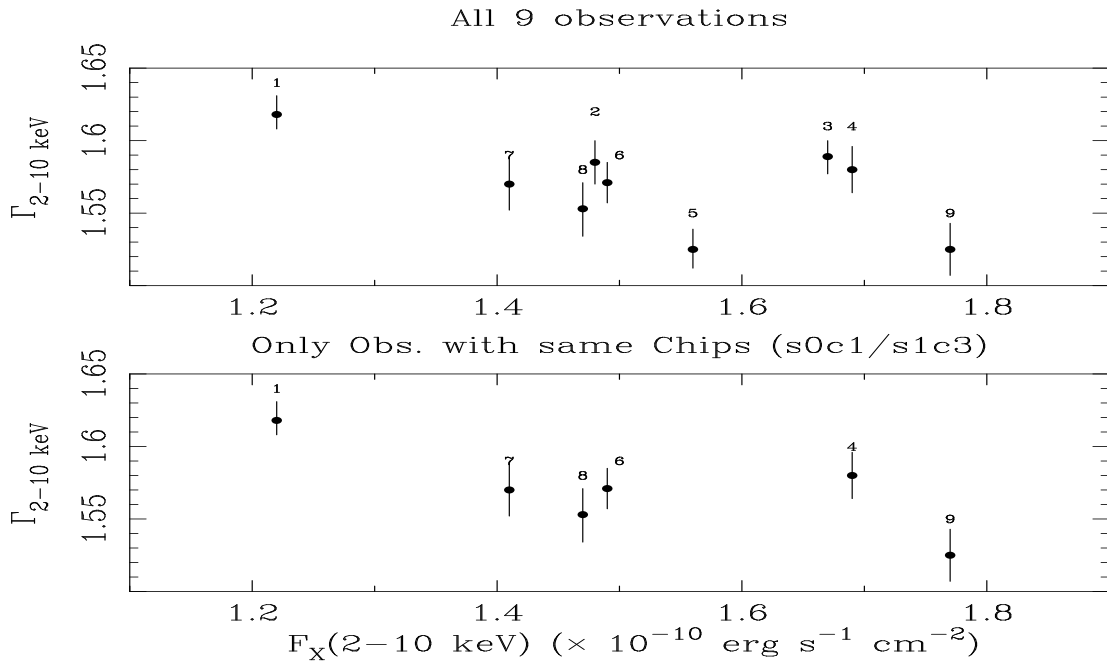


Fig. 4.— 2–10 keV photon index vs. observed 2–10 keV flux. The SIS spectra were fitted assuming a power law model with Galactic absorption. Errors are at 90% confidence for one interesting parameter.

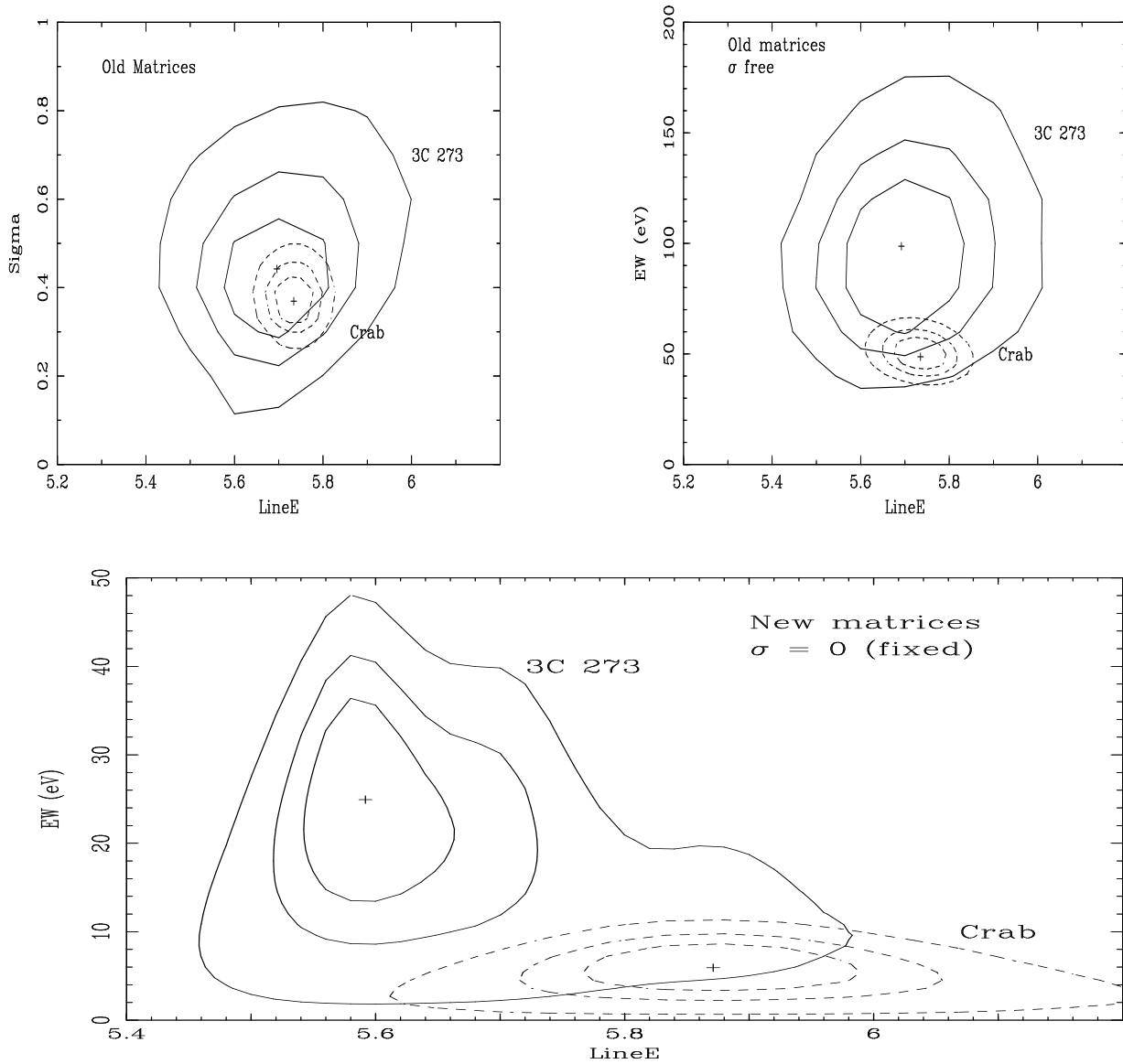


Fig. 5.— 68%, 90% and 99% confidence contour levels of 3C 273 during observation 1 (solid line) and Crab GIS spectrum (dashed line) for the Fe K width vs. energy (upper left panel) and Fe K equivalent width vs. energy (upper right panel) with the “old” *ASCA* calibrations (see text for details). The lower panel shows the Fe K equivalent width vs. energy contours for the same observation but with the latest available calibration. In this case, only upper limits were obtained for the line widths which were thus fixed to 0 eV. Note the large differences in the best-fit results between the two calibrations. Note also that the elongated shape of the 99% confidence line contours in 3C 273 (lower panel) indicates that, even with the latest calibration matrices that largely corrected for the artificial  $E \sim 5.6\text{--}5.8$  keV line in the Crab spectrum, it is sensitive to a very weak ( $EW \sim 6\text{--}7$  eV) line feature apparently still remaining in the Crab data. This suggests that no more strong calibration uncertainties should affect the measured line in 3C 273, thus strengthening our conclusion that the line is likely to be real.



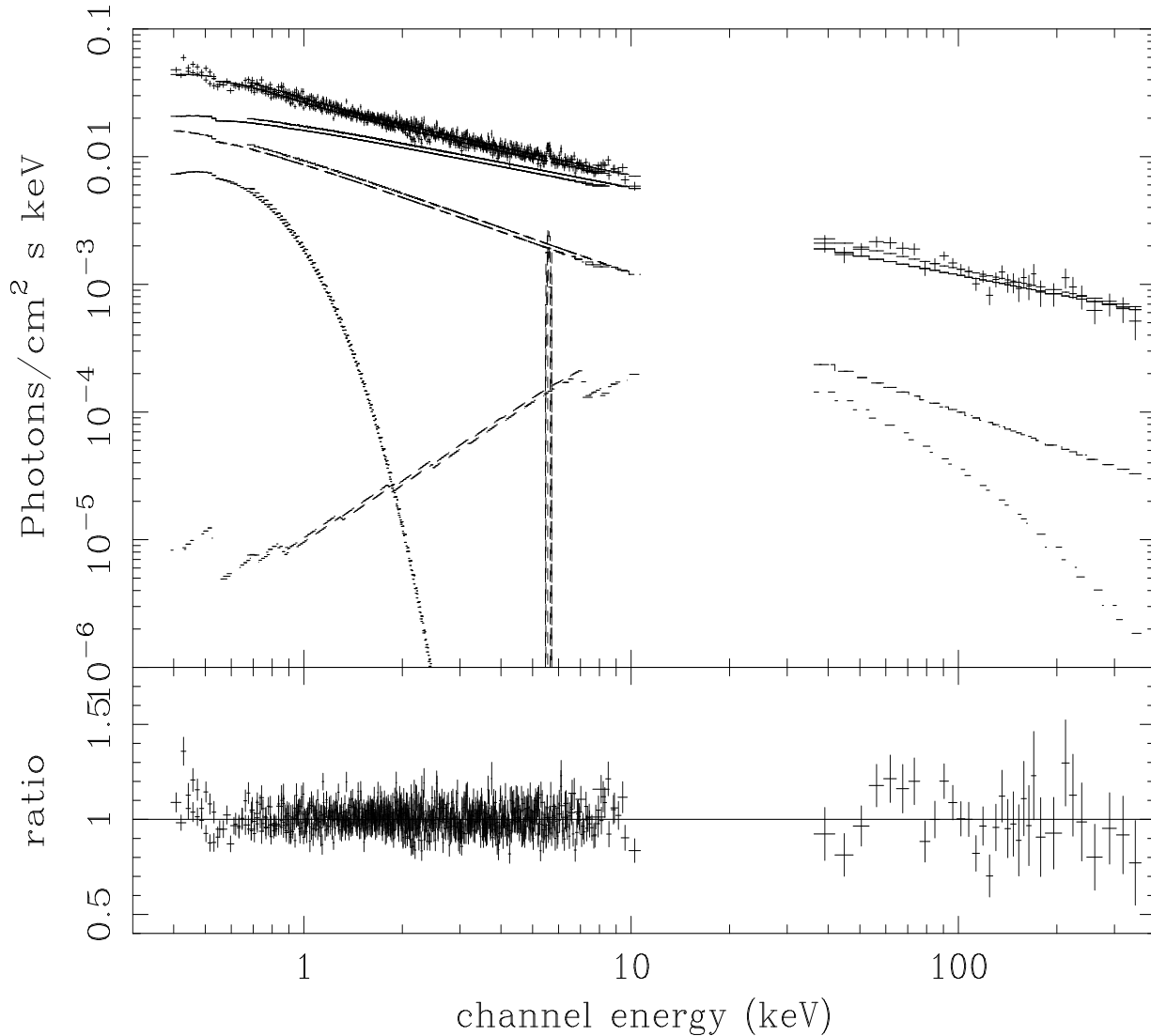


Fig. 6.— The figure shows the 0.4–300 keV unfolded spectrum and data/model ratios for a fit of an *ASCA* (observation 1) plus *OSSE* (viewing period n.3, Johnson et al. 1995) non-simultaneous data. The figure *illustrates* what could be the various components that contribute to the X-ray emission in 3C 273, i.e. a  $\Gamma \sim 1.5$ -1.6 power law (most likely due to jet radiation) plus a “Seyfert-like” spectrum consisting of a soft X-ray black-body, a  $\Gamma \sim 1.9$  power law plus a reflection component (with  $R=1$ ) and associated iron line ( $EW=150$  eV with respect to the Seyfert continuum). When the jet continuum is in a low state (like during observations 1 and 7), the features from the Seyfert contribution are more easily seen. Note that the relative normalizations of the two instruments were free to vary.